AD-A120 770 GRAIN REFINING AND MICROSTRUCTURAL MODIFICATION DURING SOLIDIFICATION(U) FLORIDA UNIV GAINESVILLE DEPT OF MATERIALS SCIENCE AND ENGINEERING G J ABBASCHIAN 1/1

UNCLASSIFIED OCT 82 N00014-81-K-0730 F/G 11/6 NL

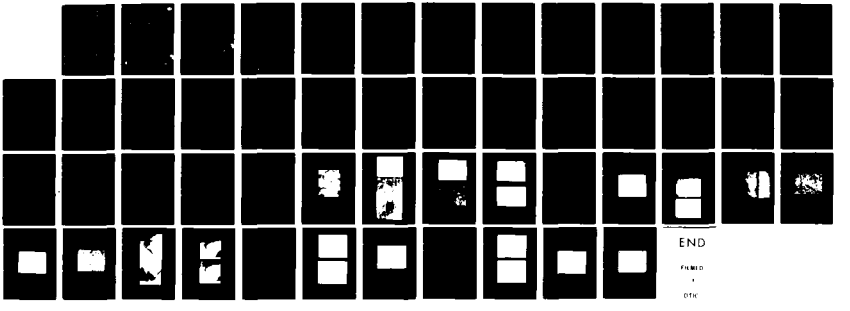

MICROCOPY RESOLUTION TEST CHART
NATIONAL BUREAU OF STANDARDS-1963-A

MICROCOPY RESOLUTION TEST CHART
NATIONAL BUREAU OF STANDARDS-1963-A

MICROCOPY RESOLUTION TEST CHART
NATIONAL BUREAU OF STANDARDS-1963-A

MICROCOPY RESOLUTION TEST CHART
NATIONAL BUREAU OF STANDARDS-1963-A

Unclassified

SECURITY CLASSIFICATION OF THIS PAGE (When Data Entered)

REPORT DOCUMENTATION PAGE	READ INSTRUCTIONS BEFORE COMPLETING FORM
1. REPORT NUMBER	2. GOVT ACCESSION NO. AD-A120 770	3. RECIPIENT'S CATALOG NUMBER
4. TITLE (and Subtitle) GRAIN REFINING AND MICROSTRUCTURAL MODIFICATION DURING SOLIDIFICATION	5. TYPE OF REPORT & PERIOD COVERED Annual Report 1 September 1981-August 1982
	6. PERFORMING ORG. REPORT NUMBER
7. AUTHOR(s) G. J. Abbaschian	8. CONTRACT OR GRANT NUMBER(s) N00014-81-K-0730; NR031-836
9. PERFORMING ORGANIZATION NAME AND ADDRESS University of Florida Department of Materials Science & Engineering Gainesville, Florida 32611	10. PROGRAM ELEMENT, PROJECT, TASK AREA & WORK UNIT NUMBERS
11. CONTROLLING OFFICE NAME AND ADDRESS Department of the Navy Materials Division - Office of Naval Research Arlington, Virginia 22217	12. REPORT DATE October 1982
	13. NUMBER OF PAGES 45
14. MONITORING AGENCY NAME & ADDRESS(if different from Controlling Office)	15. SECURITY CLASS. (of this report) Unclassified
	15a. DECLASSIFICATION/DOWNGRADING SCHEDULE

16. DISTRIBUTION STATEMENT (of this Report)

Approved for public release; distribution unlimited. Reproduction in whole or in part is permitted for any purpose of the United States government.

17. DISTRIBUTION STATEMENT (of the abstract entered in Block 20, if different from Report)

18. SUPPLEMENTARY NOTES

19. KEY WORDS (Continue on reverse side if necessary and identify by block number)

Grain refining, microstructure, solidification, supercooling, solute distribution, Cu-Fe alloys, Ni-Cr alloys, and Fe-Ni alloys.

20. ABSTRACT (Continue on reverse side if necessary and identify by block number)

This is the first annual report of a three-year research program initiated in the Materials Science and Engineering department of the University of Florida. The objective of the program is to study grain refining and microstructural modification during solidification, as affected by supercooling, the solidification rate, and/or inoculation. The experimental technique consists of using an electromagnetic levitation technique to melt one gram samples, followed by rapid solidification of the superheated or supercooled sample in a

DD FORM 1 JAN 73 1473 EDITION OF 1 NOV 65 IS OBSOLETE S/N 0102-014-6601

Unclassified

SECURITY CLASSIFICATION OF THIS PAGE (When Data Entered)

in a quenchant. The research activities so far have been concentrated in the following areas: (1) grain refining via peritectic reaction in Cu-Fe alloys, (2) microstructure and solute distribution in highly-supercooled Fe-Ni alloys, and (3) supercooling and microstructure of Cr, Ni and Cr-Ni alloys.

For Cu-Fe alloys, it has been observed that the addition of iron progressively reduces the grain size of the copper in alloys up to 2.8 w/o Fe, the minimum concentration necessary for the peritectic reaction. In the hyperperitectic alloys, where iron is the primary phase, increasing the iron concentration does not seem to influence the grain size appreciably. However, the cooling rate through the solid-liquid range above the peritectic temperature and coarsening of primary iron particles seem to have a major effect on the grain size.

For the Fe-Ni system, the effects of supercooling and rapid quenching in molten lead on the microstructure of Fe-25% Ni were studied. The solute distribution of the supercooled samples was determined by utilizing an analytical electron microscope. Similar to the results of the previous experiments, the sub-grain segragation patterns were found to be either dendritic, spherical, or a combination of the two. At supercoolings less than about 175 K, all three morphologies were observed. At larger supercoolings, however, the spherical morphology tended to predominate. Other novel structures were also noted at the larger supercoolings. The dendritic and spherical elements contained at least one region with high solute concentration, formed by partitionless solidification. The solute rich core was then surrounded by a thin shell of lower solute concentration, beyond which the nickel concentration increased to a maximum at the periphery of the elements.

For Cr-Ni system, a series of experiments were initiated on supercooling and structure of Cr, Ni, and various binary alloys of Ni-Cr. For high purity nickel and chromium, the maximum supercoolings obtained were 340 and 180 K, respectively. Primary and secondary supercooling were also observed during solidification of the binary alloys. The grain size of high purity nickel was found to decrease as the supercooling increased from 0 to 305 K. At low supercoolings, the grains tended to have nonuniform - oblong shapes, while at larger supercooling they tended to become more uniform and equiaxed. Beyond about 200 K supercooling, various fine-grained zones, interdispersed among the larger grains, were observed. The structure of the alloys which solidified at the levitated state consisted of broken primary dendrites in a eutectic matrix. The dendrite breakage is caused by the fluid flow induced by the electromagnetic field.

Technical Report No. 1
Contract N00014-81-K-0730; NR031-836

GRAIN REFINING AND MICROSTRUCTURAL MODIFICATION DURING SOLIDIFICATION

G. J. Abbaschian
Department of Materials Science and Engineering
University of Florida
Gainesville, FL 32611

15 October 1982

Annual Report for Period 1 September 1981-31 August 1982

OFFICE OF NAVAL RESEARCH
Materials Division
800 N. Quincy Street
Arlington, VA 22217

FOREWARD

This research was supported by the Office of Naval Research, Arlington, Virginia, under contract number N00014-81-K-0730. The scientific officer monitoring the program was Dr. Bruce A. MacDonald. Contribution from German Amaya, David D. McDevitt, and Joseph A. Patchett are gratefully acknowledged. Special thanks are due to Professor John Hren and the staff of the Analytical Instrumentation Center for their assistance in the electron microscopy work.

TABLE OF CONTENTS

ABSTRACT

This is the first annual report of a three-year research program initiated in the Materials Science and Engineering department of the University of Florida. The objective of the program is to study grain refining and microstructural modification during solidification, as affected by supercooling, the solidification rate, and/or inoculation. The experimental technique consists of using an electromagnetic levitation technique to melt one gram samples, followed by rapid solidification of the superheated or supercooled sample in a quenchant. The research activities so far have been concentrated in the following areas: (1) grain refining via peritectic reaction in Cu-Fe alloys, (2) microstructure and solute distribution in highly-supercooled Fe-Ni alloys, and (3) supercooling and microstructure of Cr, Ni and Cr-Ni alloys.

For Cu-Fe alloys, it has been observed that the addition of iron progressively reduces the grain size of the copper in alloys up to 2.8 w/o Fe, the minmum concentration necessary for the peritectic reaction. In the hyperperitectic alloys, where iron is the primary phase, increasing the iron concentration does not seem to influence the grain size appreciably. However, the cooling rate through the solid-liquid range above the peritectic temperature and coarsening of primary iron particles seem to have a major effect on the grain size.

For the Fe-Ni system, the effects of supercooling and rapid quenching in molten lead on the microstructure of Fe-25% Ni were studied. The solute distribution of the supercooled samples was determined by utilizing an analytical electron microscope. Similar to the results of the

previous experiments, the sub-grain segragation patterns were found to be either dendritic, spherical, or a combination of the two. At supercoolings less than about 175 K, all three morphologies were observed. At larger superoolings, however, the spherical morphology tended to predominate. Other novel structures were also noted at the larger supercoolings. The dendritic and spherical elements contained at least one region with high solute concentration, formed by partitionless solidification. The solute rich core was then surrounded by a thin shell of lower solute concentration, beyond which the nickel concentration increased to a maximum at the periphery of the elements.

For Cr-Ni system, a series of experiments were initiated on supercooling and structure of Cr, Ni, and various binary alloys of Ni-Cr. For high purity nickel and chromium, the maximum supercoolings obtained were 340 and 180 K, respectively. Primary and secondary supercooling were also observed during solidification of the binary alloys. The grain size of high purity nickel was found to decrease as the supercooling increased from 0 to 305 K. At low supercoolings, the grains tended to have nonuniform - oblong shapes, while at larger supercooling they tended to become more uniform and equiaxed. Beyond about 200 K supercooling, various fine-grained zones, interdispersed among the larger grains, were observed. The structure of the alloys which solidified at the levitated state consisted of broken primary dendrites in a eutectic matrix. The dendrite breakage is caused by the fluid flow induced by the electromagnetic field.

I. INTRODUCTION

The microstructure of a cast alloy is of great importance since many of the alloy properties are directly related to the size, shape and distribution of the grains. Fine-grained structures generally have improved low temperature strength and toughness, reduced anisotropy, better heat treatment response, reduced hot tearing tendency, and/or improved casting surface quality. The micro- and macrosegregation of the constituents also depend on the grain morphology, as well as on the solidification conditions.

Commercial grain refining during solidification is generally achieved by way of increased heterogeneous nucleation sites and/or grain multiplication, via controlling thermal, mechanical, and/or chemical conditions. Thermal controls consist of increasing the rate of heat removal via chill casting or any of the recently developed rapid solidification techniques.[1-2] Mechanical controls include magnetic stirring,[3-5] ultrasonic vibration,[6-8] vibration or rotation of the mold,[9-12] or mechanical stirring of the solidifying alloy.[13-14] The last method of grain refinement involves the addition of inoculants or alloying elements that act either as catalysts for heterogeneous nucleation or as growth inhilitors.[15-18] A typical example of this method is the use of peritectic reactions for grain refining of various commercial aluminum alloys by adding Ti and B. The addition of Ti and B presumably results in the formation of a stable (Ti, Al)B_2 peritectic compound, which provides an ideal site for subsequent heterogeneous nucleation of the aluminum phase. In general, there are distinct advantages to grain refine-

ment via peritectics in aluminum alloys. One is that the amount of alloying elements required is generally low, in the range of 0.05% TiB_2.

It seems likely that peritectic reactions can also be utilized in grain refinement of other non-ferrous or ferrous alloys. A good candidate for such investigation is Cu, which has peritectic type phase diagram with Fe, Co, V and Nb. In these systems, the amount of the additives required for peritectic reactions is small enough so as not to significantly affect the electrical conductivity of the matrix. In addition to grain refinement,[19] solid state precipitation hardening of the partially supersaturated primary phase can further improve the mechanical properties. The results of the present study on the effect of Fe on the grain size of Cu is discussed later in this report.

Supercooling prior to solidification also affects the structure and homogeneity of castings. A more obvious effect of supercooling is grain refinement caused by an increased nucleation rate. Another effect, and possibly a more important one, is grain refinement due to dendrite fragmentation during recalescence.[20,21] Each fragment, if it does not remelt completely, results in the formation of a grain. When solidification of a supercooled liquid is combined with rapid rate of heat removal, the dendrites which form below the solidus may not have enough time to disintegrate. The resulting microstructure in this case will be similar to regular dendritic structures, but with a reversed coring--the center of the dendrite will contain higher solute than the surrounding areas.[20,21] However, the mechanisms of solidification and partitioning of supercooled liquids are not well understood yet. More quantitative

analysis is required to obtain the exact concentration profile as a function of process variables. In the present study, research has been initiated to determine solute distribution in highly supercooled alloys by using STEM.

Heat and fluid conditions during solidification can also cause grain multiplications. Thermal and flow conditions can cause breakage or melting at the root of dendrite arms where the solute concentration is higher than in the other parts. When carried away, the separated arms can then resolidify, sometimes after partial remelting, leading to formation of new grains. Fluid flow, laminar or turbulent, can arise from natural convection caused by thermal or concentration gradient, from the pouring momentum in small castings, and/or from externally applied forces. Electromagnetic stirring is being commercially used to control grain size during casting of superalloys. The effect of electromagnetic stirring on the structure is also of great importance during continuous casting where an electromagnetic field is utilized to confine the liquid metal. In the experiments described later, the effect of electromagnetic stirring on the structure of Cr-Ni is shown.

The goal of this research is to study grain refining and microstructural modification in various alloys as affected by supercooling, solidification rate, inoculation, and/or peritectic reactions. The experimental technique consists of using electromagnetic levitation to melt, superheat or supercool the samples which are then quenched in water or molten lead. The program during the first year, as described in detail later, has been concentrated in the following three areas:

(1) grain refining via peritectic reaction in Cu-Fe alloys, (2) microstructure and solute distribution in highly-supercooled Fe-Ni alloys, and (3) supercooling and microstructure of Cr, Ni and Cr-Ni alloys.

II. EXPERIMENTAL PROCEDURE

The levitation apparatus used in this study, as schematically shown in Figure 1, consisted mainly of a levitation coil, a two-color pyrometer, a gas purifying system, and a quenching medium. The levitation coil consisted of a copper tube wound to have a gap between the upper and the lower turns with the upper turns wound in reverse direction to the lower. A photograph of the levitation chamber is shown in Figure 2. The coil was powered by a 450 KC, 10 KW high frequency generator. The temeprature of the levitated samples was measured and continuously monitored by a two-color pyrometer manufactured by Capentec company. The pyrometer reading is calibrated against the melting points of pure iron, nickel and copper.

High purity helium, argon, and/or hellium-2% hydrogen was continuously passed through the glass tube surrounding the sample in order to provide cooling and to prevent oxidation. The inert gases were purified by passsing through a "gas purifier," manufactured by Centorr, which utilizes titanium at 800°C as a "getter". The oxygen content of the purified gas was continuously monitored to be in the range of 10^{-19} ppm. The hellium-hydrogen gas mixture was passed through an "oxygen excavenger", which catalytically converts residual oxygen into water, and then through a liquid nitrogen trap.

The samples, each weighing about one gram, was prepared from high purity nickel (99.99%), high purity iron (99.98%), copper (99.99 and 99.999%), and/or chromium (99.95%) in a vacuum arc melting furnace in an argon atmosphere. A titanium getter was melted prior to melting of the samples.

A samples, as prepared, was lowered into the levitation coil using a platinum wire which was pulled out of the field as soon as the solid sample levitated. The gas flow and the power input to the coil were adjusted to melt and superheat the sample by about 300 K. In order to measure the maximum attainable supercooling, the sample was then cooled at a rate of 5-30 KS^{-1} until nucleation and recalescence took place. After recording the nucleation temperature, the sample was reheated, and the procedure was repeated several times. The sample was finally cooled to a desired temperature where it was allowed to solidify at the levitated state or to fall into quenching bath placed beneath the levitation chamber. The quenching media consisted of water or molten lead at 650 K.

III. RESULTS AND DISCUSSION

(a) Cu-Fe system

The nominal compositions of the alloys used to study the effect of iron additions on the grain size and microstructure of Cu are given in Table 1. The copper rich side of Cu-Fe phase diagram, contains a peritectic reaction. The minimum iron concentration necessary for the peritectic reaction in about 2.8% Fe. The alloys containing less than 2.8% Fe are termed hypoperitectic, while those containing larger amounts of iron are termed hyperperitectic alloys.

The structure of three hypoperitectic samples is shown in Figure 3. The samples were sollidified at the levitated state by cooling to 1320 K, at a rate of 30 K/S, at which temperature they were quenched in water. In general, the grain size of the hypoperitectic alloys decreases with increased iron content until a minimum is reached at about 2.86 w/o Fe. At this composition, there seems to be a slight increase in the grain size as the composition passes to the hyperperitectic region, see Figure 4. Beyond this composition, the average grain size does not seem to depend on the iron content, as shown in Figure 5. The average grain size, measured by the method of linear intercepts, as a function of iron content is shown in Figure 6.

It should be noted that the grain size of the hyperperitectic alloys is strongly influenced by the cooling rate in the solid-liquid range above the peritectic temperature. The effect can be clearly seen by comparing the structures shown in Figures 5b and 7; in the former figure, the sample was solidified at a cooling rate of 30 K/sec before quenching at 1320 K in water, while in the latter one, the sample was quenched at its liquidus. Visual observation of the samples during the slow cooling indicated that some of the iron phase, which comes out of the solution first, segregates to the surface of the droplet in the form of small patches and dendrites. The iron particles then agglomerate, forming a large patch. The rejection of iron to the droplet surface is caused by the differences in the densitites and surface energies, and fluid flow induced by the electromagnetic field.

As a result of coarsening in the solid-liquid range and/or agglomeration, the effectiveness of iron in the grain size reduction is diminished in the hyperperitectic alloys. This observation could possibly explain the nature of the fading phenomenon observed in grain refining via peritectic reactions. In our experiments, however, the electromagnetic field may have accelerated the fading process.

Future work on grain refining of copper will include: (a) effect of iron on grain size of rapidly quenched samples, (b) effect of V, Co and Nb on the grain size, (c) STEM analysis of composition profiles, and (d) solidification mechanism in peritectic systems.

(b) Fe-25% Ni system

Similar to previous studies,[20] the microstructure of Fe-25% Ni samples as a function of supercooling was found to fall into three major categories: dendritic, spherical, or a combination of the two. At supercoolings less than about 175 K, all three morphologies were observed. At supercoolings exceeding this value, however, the spherical morphology tended to predominate. Typical examples of dendritic, spherical, and mixed microstructures are shown in Figures 8a-c for three samples were supercooled before quenching to 175, 195 and 0 K, respectively. In addition to the spherical morphology, other segregation patterns were noted at large supercoolings. For example, microstructures of three samples which were supercooled 220 K before quenching in molten lead are shown in Figure 9. The structure shown in Figure 9a is a fine scale spherical morphology, while that of Figure 9b is a coarse segregation pattern with a preponderance of Widmanstatten plates. Several cracks

are also visible in the structure. Figure 9c is a "rosette" structure which has a radiating fan appearance with elongated cells emanating from central hubs.

The spherical shape which predominates at supercoolings exceeding 175 K is believed to be due to fragmentation of the dendrites in the early stages of solidification. If the fragements do not remelt or agglomerate but continue growing independently as solidification continues, the spherical morphology will result. Fragmentation can be caused by fluid flow driven by solidification shrinkage, thermal gradients, and/or agitation from free falling or interaction with the quenchant.

The metallographic examination further revealed the presence of a fine dendritic segregation pattern within the larger dendrites, as shown in Figure 10. Surrounding the solute-rich "primary" dendrites is a lightly colored solute-poor region which gradually darkens toward the edge of the larger dendrite arms. In general, there is a single primary dendrite arm within each larger arm. In some areas, however, several primary arms are present within a larger arm, as can be seen in Fig. 11 which shows a scanning electron microscope image of dendrites.

Samples having the spherical segregation pattern also exhibited solute rich cores in the middle of each element as shown in Figure 12. However, the solute-rich primary cores are not fully developed dendrites but have a simple cross shape. The crosses are surrounded by a lightly colored, solute-poor region, darkening toward the edge of the spherical elements.

A JOEL 200 scanning transmission electron microscope was used to obtain accurate chemical analysis measurements on a fine scale. Thin samples were prepared by slicing the droplets with a diamond saw followed by electrochemical thinning in a solution of 90% acetic- 10% perchloric acid at 280 K. Figure 13a is a scanning transmission micrograph of a spherical element similar to the ones shown in Figure 12. A cell containing a dark cross is visible next to the very light area which is a hole in the sample. The gray areas surrounding the cross reveal portions of the sample which have been selectively etched and thinned. The contrast can be color enhanced with the aid of a computer as shown in Figure 13b. The image in this Figure is the same as that of Figure 13a only rotated during image processing.

Iron and nickel X-ray maps of the region are shown in Figures 14a and b, respectively. The maps indicate there are fewer counts of both elements in the area surrounding the cross. Similarly high elemental counts of both elements were obtained at the cross and cell boundary. Since the variation in the number of counts obtained is greatly influenced by thickness variations in the sample, individual elemental X-ray maps may give a misleading impression of the distribution of elements. However, by simultaneously collecting both iron and nickel signals at any given position and using the ratio of the counts, more accurate compositional measurements can be made. The following equation was used to relate measured X-ray intensities to concentrations:

$$\frac{C_{Ni}}{C_{Fe}} = k \frac{I_{Ni}}{I_{Fe}}$$

where C_{Ni} is the calculated Ni concentration, C_{Fe} is the calculated Fe concentration, K is a constant, I_{Ni} is the intensity of the Ni Kα peak, and I_{Fe} is the intensity of the Fe Kα peak. The thin film criteria was assumed to apply so thickness and absorption factors were not considered. The value of k was calculated to be 1.7 by assuming the central cross to have a nickel concentration of 25%. Ratios of the X-ray intensitites were obtained at several positions across the cell.

Calculated concentrations versus position across a cell using the above equation are given in Figure 15. The nickel concentration in the solute-poor area surrounding the cross is approximately 23.8% Ni. Beyond this area, the nickel concentration gradually increases to approximately 31% Ni at the edge of the cell. It should be noted that if adsorption factors are accounted for they would tend to exaggerate the differences between the maximum and minimum concentrations. This area is presently under investigation in order to obtain a more accurate chemical analysis.

The solute distribution in supercooled samples are considerably different from samples without supercooling. For non-supercooled samples, the minimum solute concentration is in the center of the dendrite arms. For supercooled samples, however, the concentration of nickel in the central portion is high, presumably of the original alloy composition. This region is surrounded by a shell of lower solute concentration which gradually increases in solute concentration as the edge of the element is approached.

The following simplified model can be given to describe solidification of an alloy supercooled to a temperature below the solidus: When nucleation occurs, the initial solid forms by an essentially diffusionless transformation and so has the composition of the original alloy. The latent heat of fusion liberated raises the temperature of the sample to a point where solute partitioning at the interface begins. The solidification then continues with the solid decreasing in solute concentration while the liquid ahead of the interface becomes enriched until the maximum recalescence temperature is reached. Beyond this, the temperature decreases again as heat is transferred to the surroundings, and the final portion solidifies similar to conventional solidification processes.

In a model proposed by Kattamis et al.,[22-24] the partitioning is assumed to occur at the solidus. Thermodynamic considerations based upon the T_o concept,[25] however, indicate that partitionless solidification may continue until the T_o temperature is reached. Above T_o temperature, which is between the liquidus and solidus, solidification must occur by partitioning if the free energy is to be decreased. Other factors such as interfacial and diffusional kinetics, non-adiabatic solidification, and remelting of the existing solid during recalescence can also influence the temperature and nature of the partitioning.

Preliminary compositional profile measurements presented in this study seem to agree qualitatively but not quantitatively with the above mentioned simplified model. However, more accurate chemical analysis is required for any quantitative comparison. The information will be in-

valuable in understanding the solidification mechanisms and solute redistribution during solidification of highly supercooled and rapidly quenched metals.

(c) Cr-Ni system

The initial research study on Cr-Ni system has been directed towards characterizing the structure of the pure components as well as four binary alloys with the compositions given in Table 2. The presently accepted phase diagram for Cr-Ni is a simple eutectic type, with a eutectic temperature and composition at 1618 K and 51 w/o Cr, respectively.[26] However, other diagrams containing a eutectoid or up to 5 phase transformations in the Cr-rich side have also been suggested.[27,28]

The maximum supercoolings attained with pure Ni and Cr were 340 and 180 K, respectively. Previously reported experiments with nickel have yielded maximum supercoolings in the range of 300-320 K.[29] No previously published data has been found on supercooling of pure Cr.

Two recalescence and thermal arrests are expected upon cooling of the binary alloys. The initial one would correspond to nucleation of the primary phase, while the second one would correspond to nucleation of the second phase from the eutectic liquid. These have been identified in our experiments and the maximum supercoolings obtained in each alloy system are given in Table 2. However, other thermal arrests on the Cr-rich side, not corresponding to any transformation predicted by the accepted phase diagram, have been observed. Microstructural studies are underway to determine the origin of these thermal arrests.

The effect of supercooling in the range of 0-305 K on the grain structure of nickel is represented in Figure 16. In general, the grains tend to have non-uniform size and shape at low supercoolings, but they become more uniform and equiaxed as the supercooling increases. When the supercoolings increase beyond 200 K, however, regions with extremely fine grains appear within the equiaxed structure, see Figure 17. The grains also show twinning at the higher supercooling.

There is also a progressive reduction in grain size with increased degree of supercooling. The average grain size of the large grains, measured by the randon intercept method detailed in ASTM E-112, shows approximately a linear relationship with the supercooling as shown in Figure 18. The finer grains that appeared at large supercoolings were about one order of magnitude smaller.

The structure of the binary alloys solidified under various conditions are shown in Figures 19 to 21. In general, the samples which were fully liquid when quenched in water, showed conventional dendrites of the primary phase surrounded by a eutectic matrix, as shown in Figure 19. On the other hand, the structure of the samples which had solidified at the levitated state prior to quenching consisted of broken primary dendrites in the eutectic matrix. Examples are shown in Figure 20 for 60 Cr-40 Ni samples which were quenched just after solidification. The primary dendrites in this figure are chronium rich. Fine-plate like solid state precipitates within the dendrites can also be seen at a higher magnification. The nature of the precipitates is being presently investigated.

The structure of the alloys which were quenched form the solid-liquid range, prior to the second recalescence, was similar to that of the samples which had completely solidified at the levitated state. An example is given in Figure 21 for a 60 Cr-40 Ni sample which was solid plus liquid when dropped at about 20 K supercooling below the solidus temperature. The primary dendrites are chronium-rich in the eutectic matrix which is not ressolved in the figure.

The fragmentation of the dendrites in the alloys which had completely or partially solidified at the levitated state is caused by the fluid flow induced by the electromagnetic field. Further studies are underway to investigate the phenomenon in more detail.

SUMMARY

The research activities during the first year have been concentrated in the following areas: (1) grain refining via peritectic reaction in Cu-Fe alloys, (2) microstructure and solute distribution in highly-supercooled Fe-Ni alloys, and (3) supercooling and microstructure of Cr, Ni and Cr-Ni alloys. The experimental technique consisted of using an electromagnetic levitation technique to melt one gram samples, followed by rapid solidification of the superheated or supercooled sample in a quenchant.

For Cu-Fe alloys, it has been observed that the addition of iron progressively reduces the grain size of the copper in alloys up to 2.8 w/o Fe, the minmum concentration necessary for the peritectic reaction. In the hyperperitectic alloys, where iron is the primary phase, increas-

ing the iron concentration does not seem to influence the grain size appreciably. However, the cooling rate through the solid-liquid range above the peritectic temperature and coarsening of primary iron particles seem to have a major effect on the grain size.

For the Fe-Ni system, the effects of supercooling and rapid quenching in molten lead on the microstructure of Fe-25% Ni were studied. The solute distribution of the supercooled samples was determined by utilizing an analytical electron microscope. Similar to the results of the previous experiments, the sub-grain segragation patterns were found to be either dendritic, spherical, or a combination of the two. At supercoolings less than about 175 K, all three morphologies were observed. At larger supercoolings, however, the spherical morphology tended to predominate. Other novel structures were also noted at the larger supercoolings. The dendritic and spherical elements contained at least one region with high solute concentration, formed by partitionless solidification. The solute rich core was then surrounded by a thin shell of lower solute concentration, beyond which the nickel concentration increased to a maximum at the periphery of the elements.

For Cr-Ni system, a series of experiments were initiated on supercooling and structure of Cr, Ni, and various binary alloys of Ni-Cr. For high purity nickel and chromium, the maximum supercoolings obtained were 340 and 180 K, respectively. Primary and secondary supercooling were also observed during solidification of the binary alloys. The grain size of high purity nickel was found to decrease as the supercooling increased from 0 to 305 K. At low supercoolings, the grains tended

to have nonuniform - oblong shapes, while at larger supercooling they tended to become more uniform and equiaxed. Beyond about 200 K supercooling, various fine-grained zones, interdispersed among the larger grains, were observed. The structure of the alloys which solidified at the levitated state consisted of broken primary dendrites in a eutectic matrix. The dendrite breakage is caused by the fluid flow induced by the electromagnetic field.

REFERENCES

1. "Rapid Solidification Processing, Principles and Technology I," Edited by R. Mehrabian, B. H. Kear, and M. Cohen, Baton Rouge, Claitor's Publishing (1977).

2. "Rapid Solidification Processing, Principles and Technology II," Edited by R. Mehrabian, B. H. Kear, and M. Cohen, Baton Rouge, Claitor's Publishing, (1980).

3. D. R. Uhlmann, T. P. Seward, III and B. Chalmers: Trans. Met. Soc. AIME, 1966, v. 236, p. 527.

4. G. S. Cole and G. F. Bolling: Trans. Met. Soc. AIME, 1966, v. 236, p. 1366.

5. F. A. Crossley: Iron Age, 1960, v. 186, p. 102.

6. D. H. Lane, J. W. Cunningham and W. A. Tiller: Trans. Met. Soc. AIME, 1960, v. 218, p. 985.

7. D. H. Lane and W. A.Tiller: Trans. Met. Soc. AIME, 1960, v. 218, p. 578.

8. A. H. Freedman and J. F. Wallace: Trans. AFS, 1957, v. 65, p. 578.

9. R. S. Richards, W. Rostoker: Trans. ASM, 1956, v. 48, p. 884.

10. R. G. Garlick and J. F. Wallace: Mod. Castings, 1959, v. 35, No. 6, p. 86.

11. R. T. Southin: J. Inst. Met., 1966, v. 94, p. 401.

12. F. A. Corsely, R. D. Fisher and A. G. Metcalfe: Trans. Met. Soc. AIME, vo. 221, p. 419.

13. D. Spencer, R. Mehrabian and M. C. Flemings: Met. Trans., 1972, v. 3, p. 1925.

14. S. D. Ramati, G. J. Abbaschian and R. Mehrabian: Met. Trans. 13, 1978, vol. 9B(2), p. 241.

15. A. Cibula: J. Inst. Met., 1949, vol. 76, p. 321.

16. J. F. Wallace: J. of Metals, 1963, vol. 15, p. 372.

17. N. Church, P. Wieser and J. F. Wallace: Modern Castings, 1966, vol. 44, p. 129.

18. G. K. Turnbull, D. M. Patton, G. W. Form and J. F. Wallace: Trans. AFS, 1961, vol. 69, p. 792.

19. A. Cibula, J. of Inst. Metals, 1953, vol. 82, p. 513.

20. G. J. Abbaschian, M. C. Fleming, "Supercooling and Structure of Levitated Fe-Ni Alloys," to be published.

21. D. D. McDevitt and G. J. Abbaschian, "Microstructure and Solute Distribution in Highly-Supercooled Fe-Ni Alloys, to be published in Microstructural Science, vol. 11.

22. T. Z. Kattamis, "Redistribution of Solute in Highly Undercooled Iron-Nickel Alloy," Z. Metalkunde, 1970, p. 856.

23. T. Z. Kattamis, W. F. Brower, and R. Mehrabian, "Microstructure and Segregation in Splat-Cooled Iron Nickel Alloy," J. Crystal Growth, 1973, vol. 19, p. 229.

24. T. Z. Kattamis, and M. C. Flemings, "Dendritic Structure and Grain Size of Undercooled Melts," Met. Trans., 1960, vol. 236, p. 1523.

25. J. C. Baker, and J. W. Cahn, "Thermodynamics of Solidification," in Solidification, an ASM publication (1971).

26. ASM Metals Handbook, vol. 8, Eighth Edition (1961).

27. C. Stein and N. J. Grant, J. of Metals, 1955, vol. 7, p. 127.

28. A. T. Grigorev, E. M. Sokolovskaya, M. V. Maksimova, I. G. Sokolova, and N. A. Nedumov, Rus. J. Inorg. Chem., 1960, vol. 5, p. 1275.

29. D. Turnbull, J. Metal, 1950, vol. 188, p. 1144.

Table I

Nominal Composition of Cu-Fe Alloys and Their Average Grain Size

Sample	Composition wt % Fe	Average Grain Size* (mm)	Remarks
A10	0.72	0.2707±.09	Hypoperitectic
A15	2.14	0.112±.03	Hypoperitectic
A 4	2.72	0.051±.008	Hypoperitectic
A41	2.86	0.042±.01	Approx. peritectic
A13	2.88	0.076±.01	Approx. peritectic
A32	3.27	0.073±.02	Hyperperitectic
A39	7.46	0.045±.01	Hyperperitectic
A20	3.12	.021±.004	Hyperperitectic

All the samples, except A20, solidified at the levitated state prior to quenching. Sample A20 was quenched in water from the liquidus temperature.

Table II

Nominal Composition of Cr-Ni Alloys
and the Maximum Supercoolings Attained

System	%Ni	%Cr	Maximum Undercoolings K	
			Primary	Secondary
Cr	--	100-	180	NA
A	90	10	15	85
B	20	80	100	NM
C	40	60	200	100
D	50	50	75	60
E	60	40	NM	NM
Ni	100	--	350	NA

NA = Not Applicable

NM = Not Measured

FIGURE CAPTIONS

Figure 1: Schematic representation of the levitation melting system.

Figure 2: Photograph of the levitation coil; the pyrometer is to the left and the quenching bath is in the lower portion beneath the coil.

Figure 3: Effect of iron on the grain size of copper: (a) 0.72% Fe, (b) 2.14% Fe, and (c) 2.72% Fe. Magnification 200X.

Figure 4: Change in the grain size as the alloy changes from hypoperitectic to hyperperitectic composition (a) 2.86% Fe at 200X and (b) 2.88% Fe at 100X magnification.

Figure 5: The effect of iron on the grains size of hyperperitectic copper alloys: (a) 3.27 wt% Fe at 100X, and (b) 7.46 wt% Fe at 200X.

Figure 6: Average grain size vs iron concentration.

Figure 7: Structure of Cu-3.12 wt% Fe quenched at 1428 K in water (magnification 200X). Note the structure fineness as compared with that of Figure 5b.

Figure 8: Microstructure of three Fe-25% Ni samples showing three categories of: (a) dendritic morphology in a sample supercooled 175 K prior to quenching in lead, (b) spherical morphology in a sample supercooled 195K prior to recalescence and lead quenching, and (c) mixed morphology in a sample quenched with zero supercooling in water. (a) at 250X, (b) at 100X and (c) at 250X.

Figure 9: Microstructure of three samples supercooled 220 K before quenching in lead: (a) fine spherical morphology, (b) coarse segregation with Widmanstatten plates and fine cracks, and (c) rosette pattern. Magnification 100X.

Figure 10: The dendritic morphology etched to reveal fine "primary" dendrites within the dendrite arms. The sample was supercooled 175 K before quenching in molten lead. Magnification 250X.

Figure 11: A SEM micrograph of the dendritic morphology where two primary crosses are within an arm are visible in the upper right corner. Magnification 1000X.

Figure 12: The spherical morphology showing dark colored solute rich crosses in the center of each element, surrounded by a solute poor region which gradually darkens toward the edge. The sample was supercooled 20 K before quenching in molten lead. Magnification 250X.

Figure 13: STEM micrographs of a spherical element similar to those of Figure 12. The hole and the thin areas of the sample are lighter in color; (a) scanning transmission micrograph and (b) computer enhanced image.

Figure 14: (a) Iron and (b) nickel Kα x-ray map of the cell shown in Figure 13. The lighter colored regions indicate higher intensity signals.

Figure 15: Approximate compositional profile across an element.

Figure 16: The grains structure of pure nickel at (a) 76K and (b) 225 K supercooling. Magnification 50X.

Figure 17: Grain structure of nickel supercooled 305 K. Magnification 100X.

Figure 18: Effect of supercooling on the average grain size of nickel samples quenched in water.

Figure 19: Dendritic-structure in two fully liquid 60 Cr-40 Ni samples quenched in water (a) at the liquidus temperature and (b) at 10 K supercooling below the liquidus. Magnification 200X.

Figure 20: Microstructure of a 60 Cr-40 Ni sample which had solidified at the levitated state prior to quenching in water. Magnification 200X.

Figure 21: Microstructure of a 60 Cr-40 Ni sample quenched at the solid plus liquid range with 15-28 K supercooling below the solidus temperature. Magnification 200X.

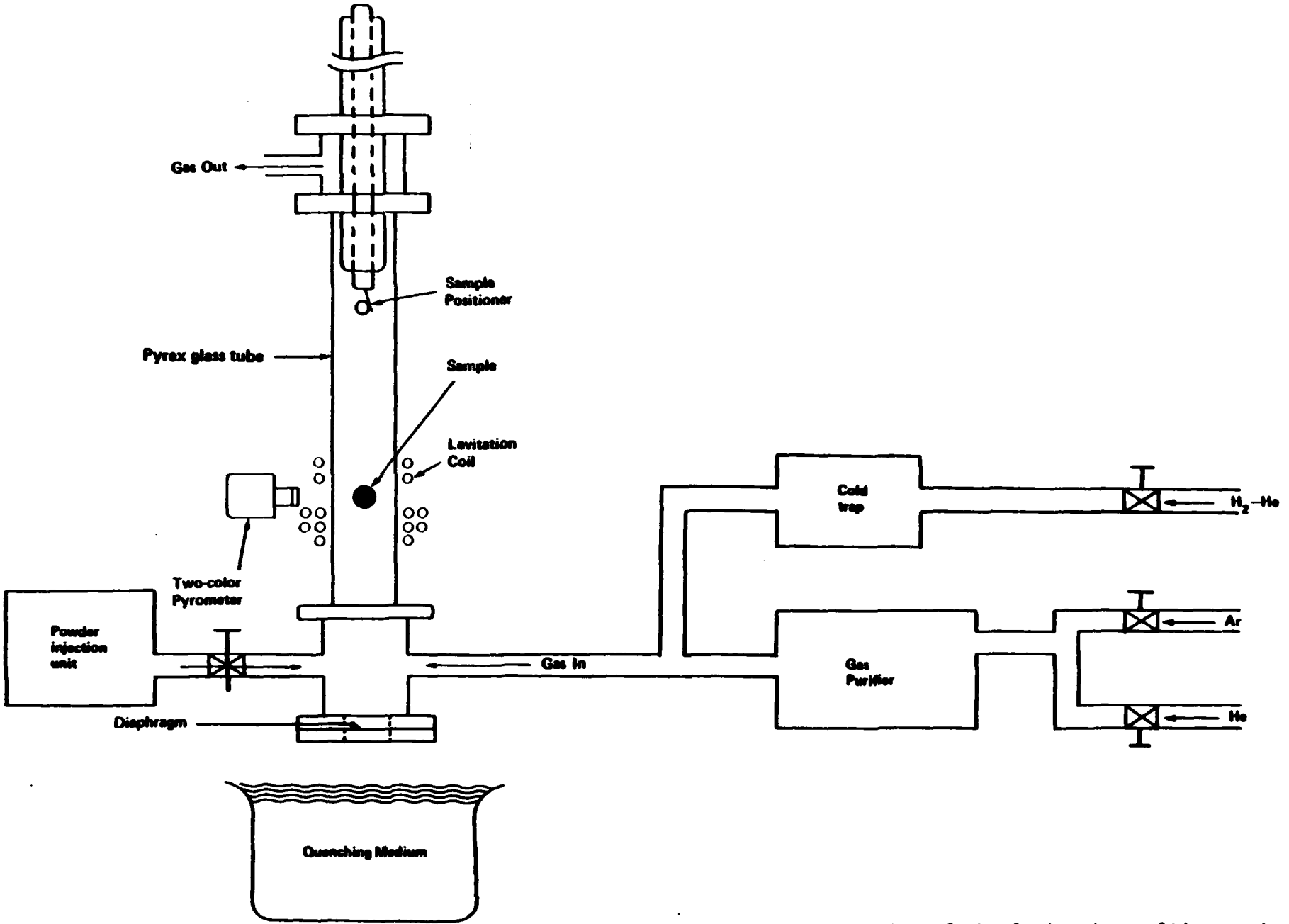

Figure 1. Schematic representation of the levitation melting system.

Figure 2. Photograph of the levitation coil; the pyrometer is to the left and the quenching bath is in the lower portion beneath the coil.

Figure 3. Effect of iron on the grain size of copper: (a) 0.72% Fe, (b) 2.14% Fe, and (c) 2.72% Fe. Magnification 200X.

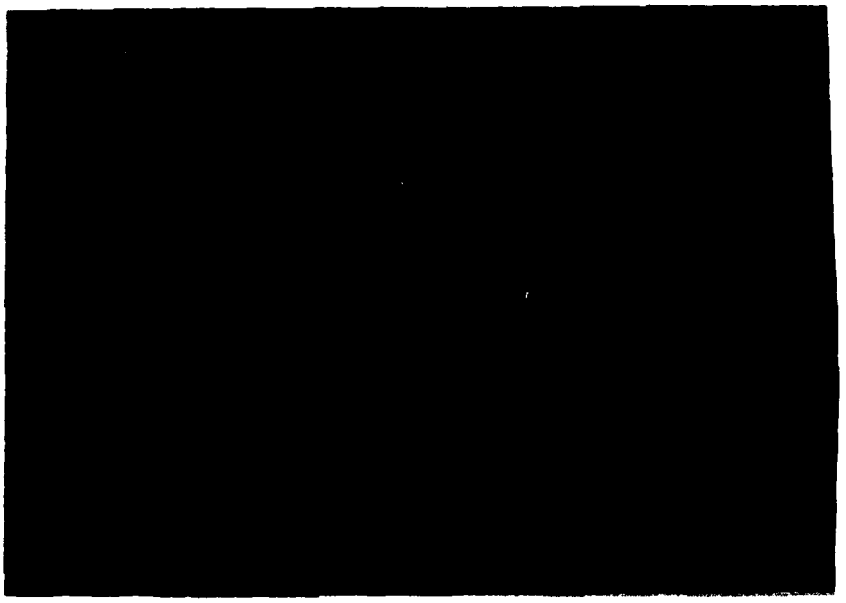

a

b

Figure 4. Change in the grain size as the alloy changes from hypoperitectic to hyperperitectic composition (a) 2.86% Fe at 200X and (b) 2.88% Fe at 100X magnification.

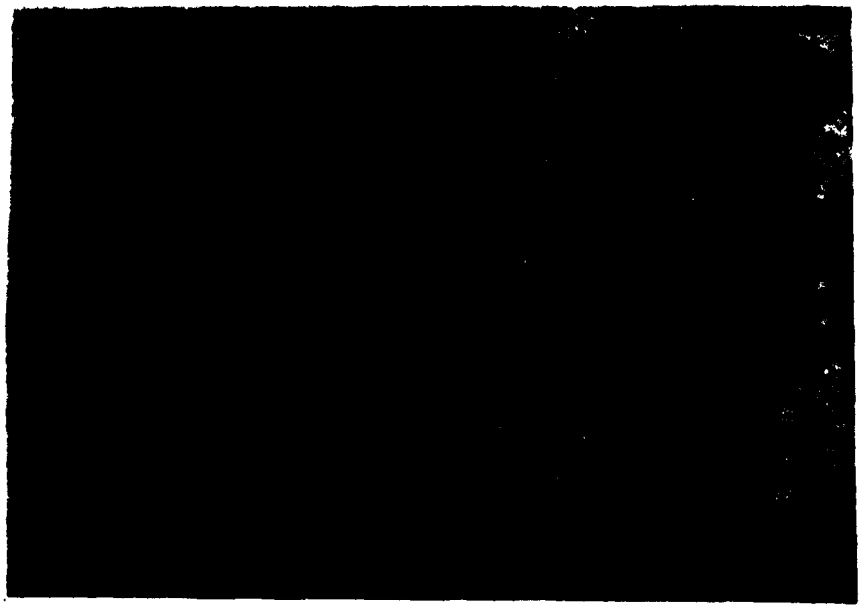

a

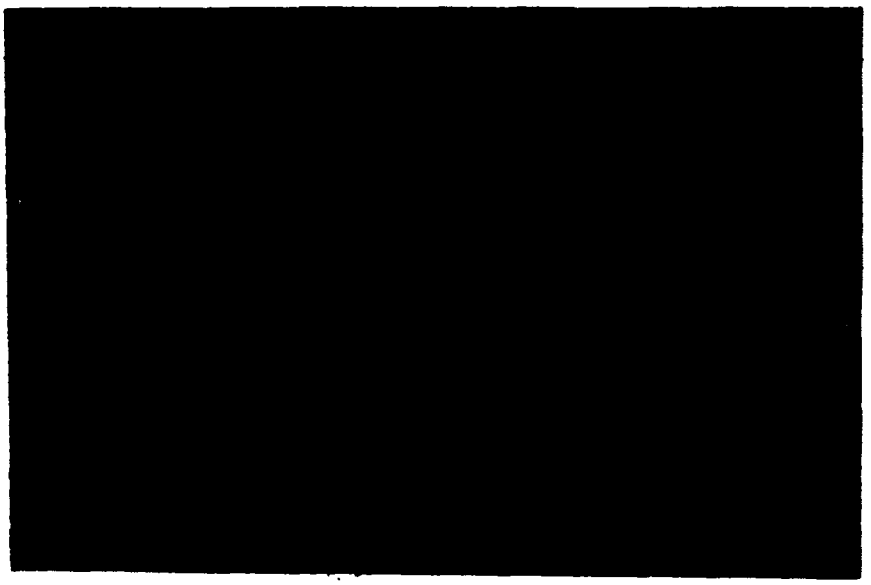

b

Figure 5. The effect of iron on the grains size of hyperperitectic copper alloys: (a) 3.27 wt% Fe at 100X, and (b) 7.46 wt% Fe at 200X.

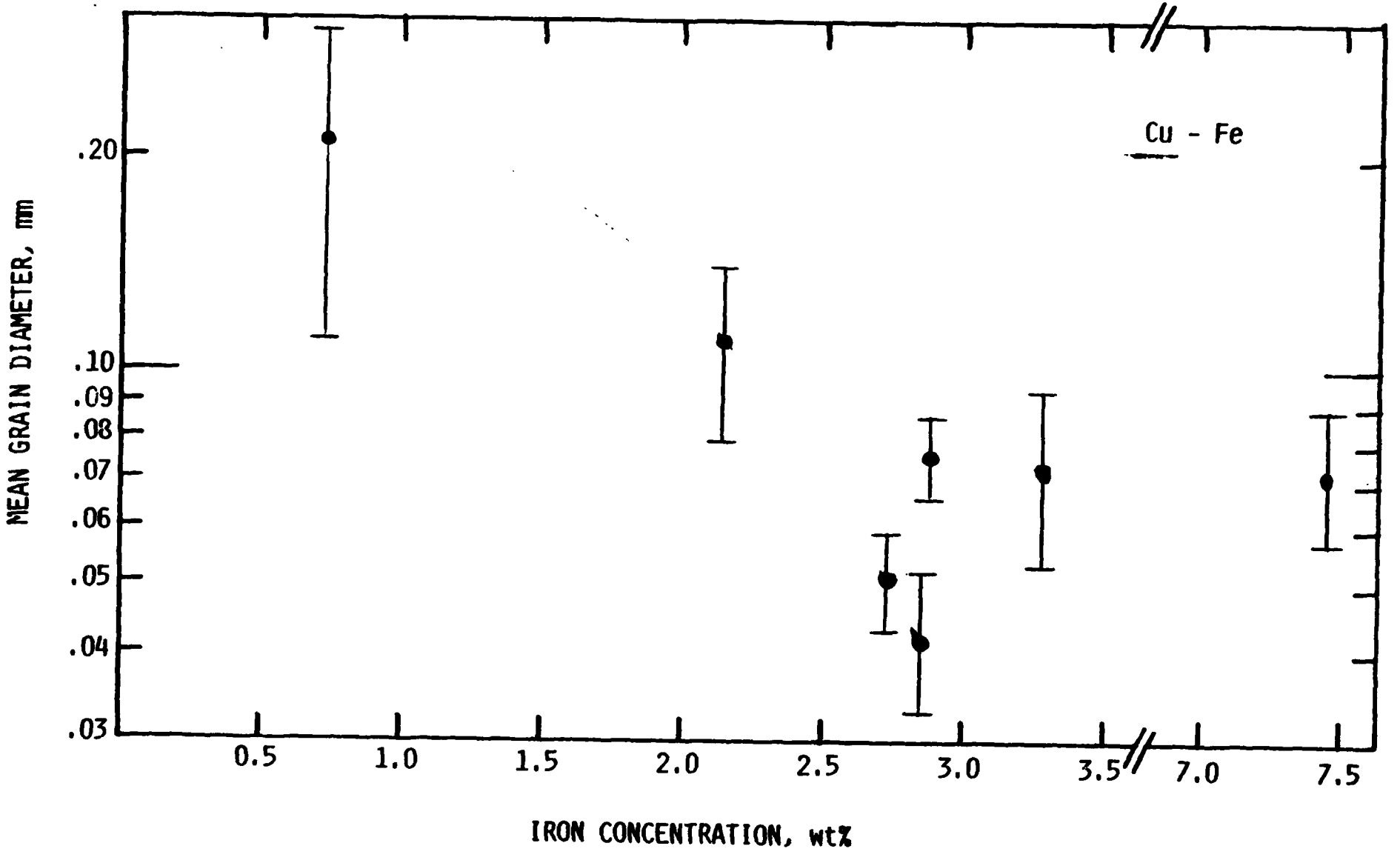

Figure 6. Average grain size vs iron concentration.

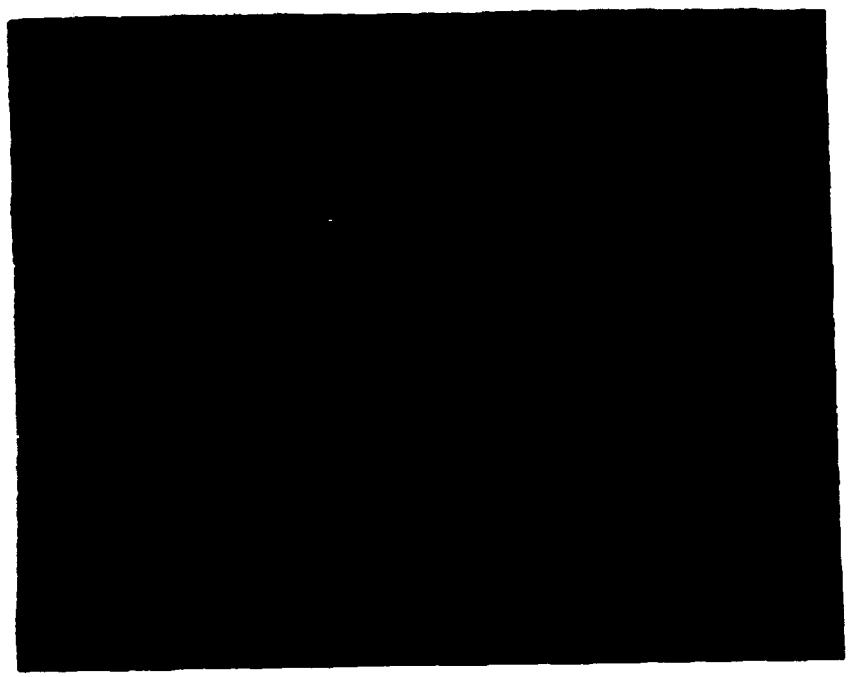

Figure 7. Structure of Cu-3.12 wt% Fe quenched at 1428 K in water (magnification 200X). Note the structure fineness as compared with that of Figure 5α.

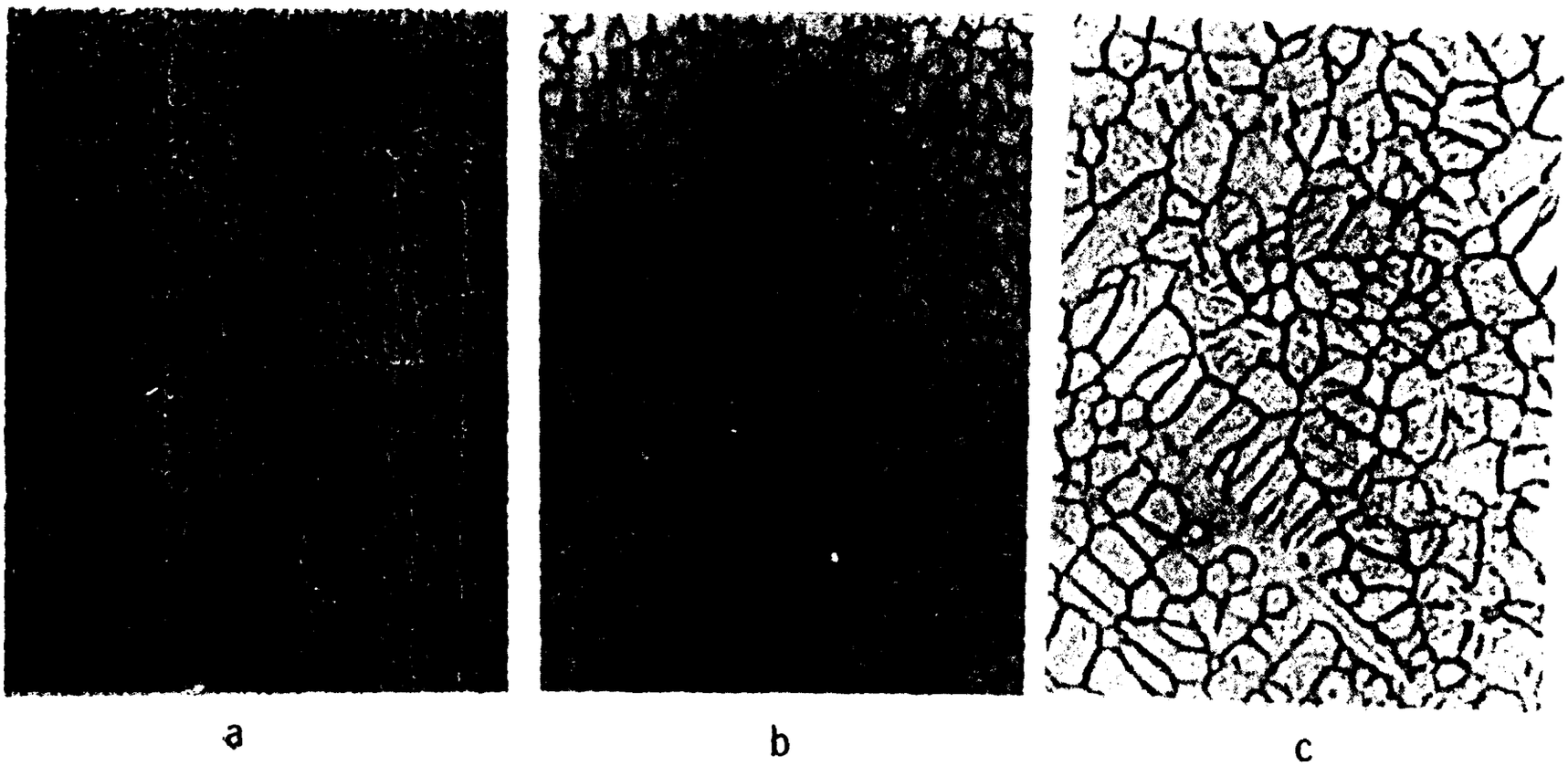

Figure 8. Microstructure of three Fe-25% Ni samples showing three categories of: (a) dendritic morphology in a sample supercooled 175 K prior to quenching in lead, (b) spherical morphology in a sample supercooled 195 K prior to recalescence and lead quenching, and (c) mixed morphology in a sample quenched with zero supercooling in water. (a) at 250X, (b) at 100X and (c) at 250X.

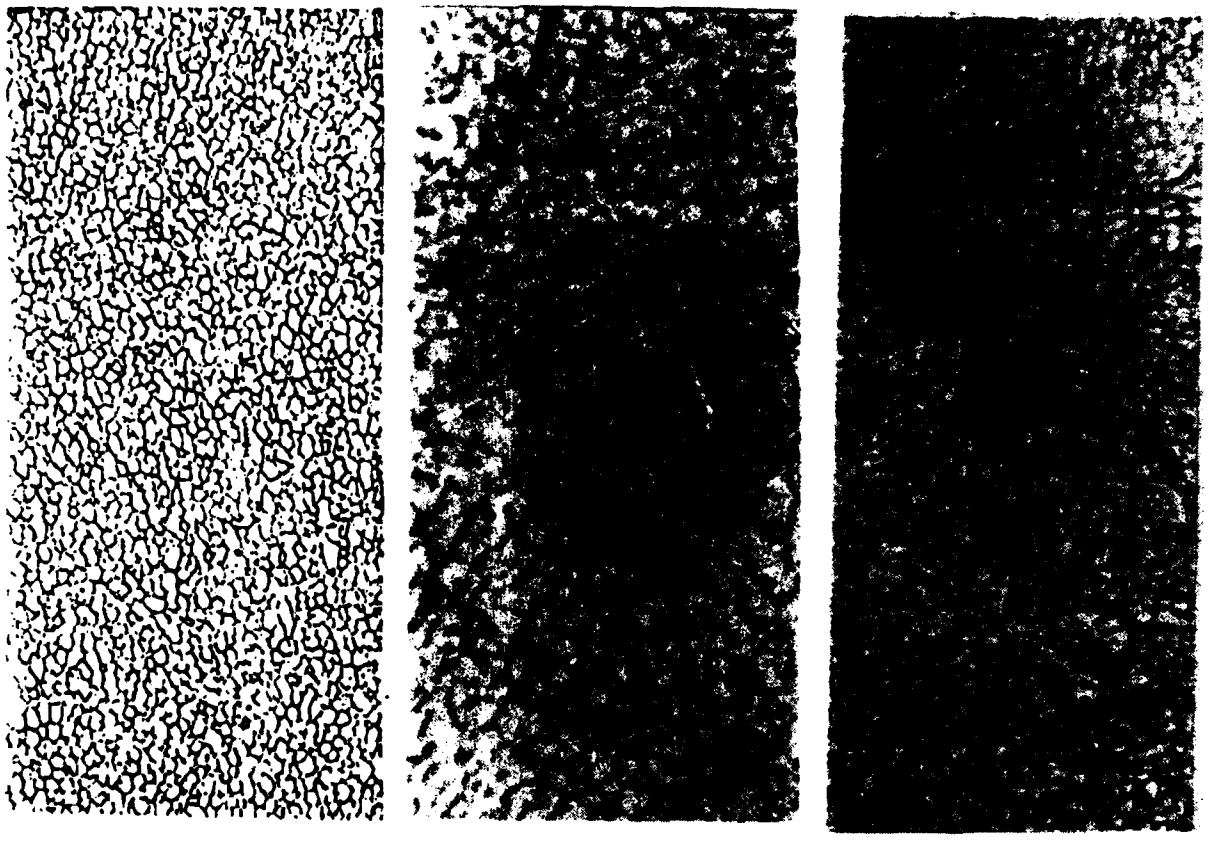

Figure 9. Microstructure of three samples supercooled 220 K before quenching in lead: (a) fine spherical morphology, (b) coarse segregation with Widmanstatten plates and fine cracks, and (c) rosette pattern. Magnification 100X.

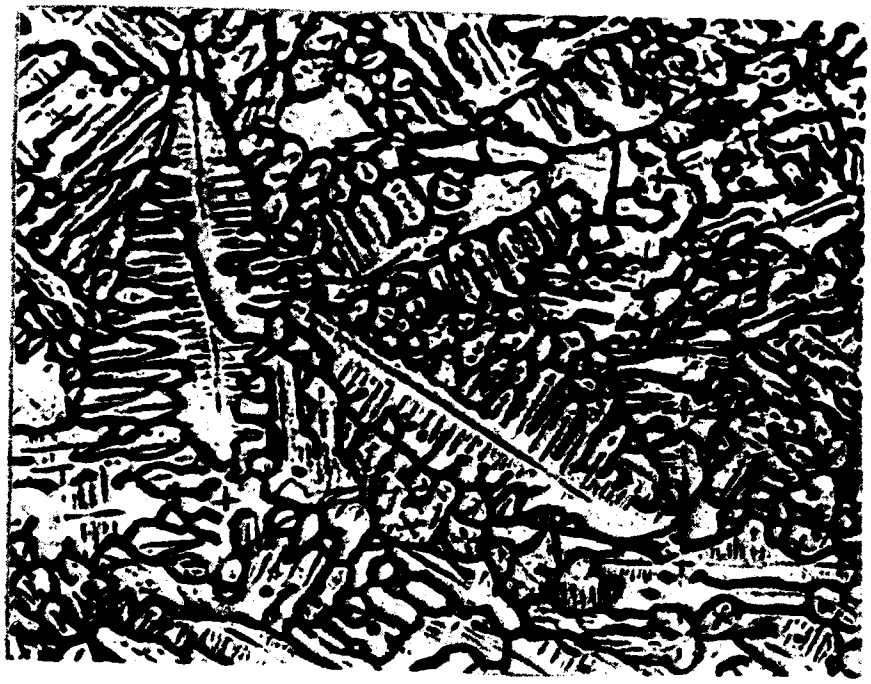

Figure 10. The dendritic morphology etched to reveal fine "primary" dendrites within the dendrite arms. The sample was supercooled 175 K before quenching in molten lead. Magnification 250X.

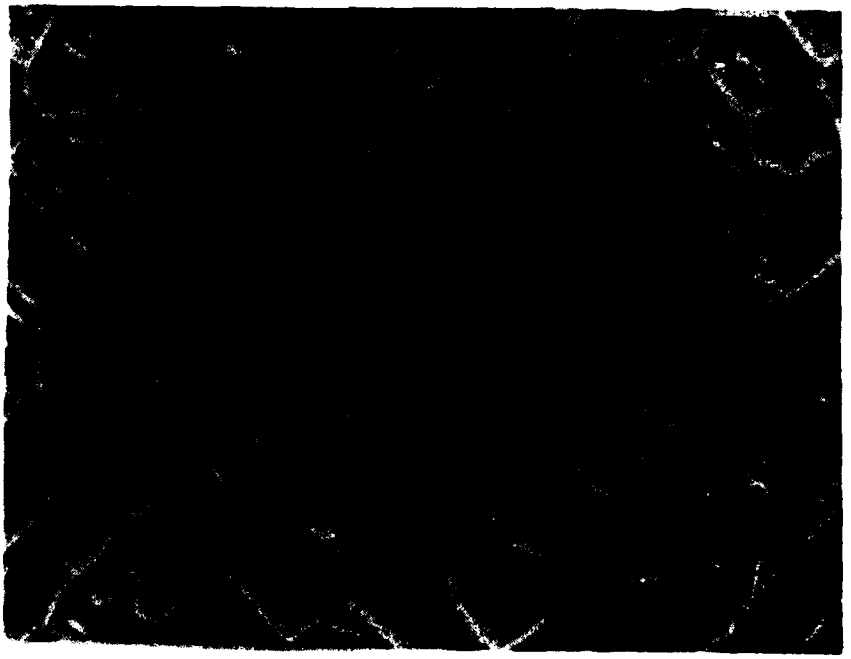

Figure 11. A SEM micrograph of the dendritic morphology where two primary crosses are within an arm are visible in the upper right corner. Magnification 1000X.

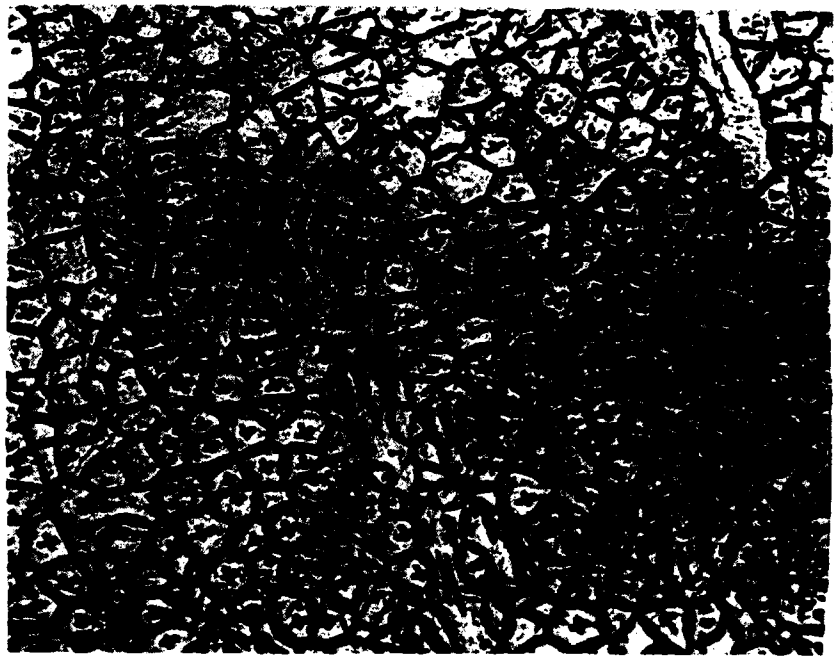

Figure 12. The spherical morphology showing dark colored solute rich crosses in the center of each element, surrounded by a solute poor region which gradually darkens toward the edge. The sample was supercooled 20 K before quenching in molten lead. Magnification 250X.

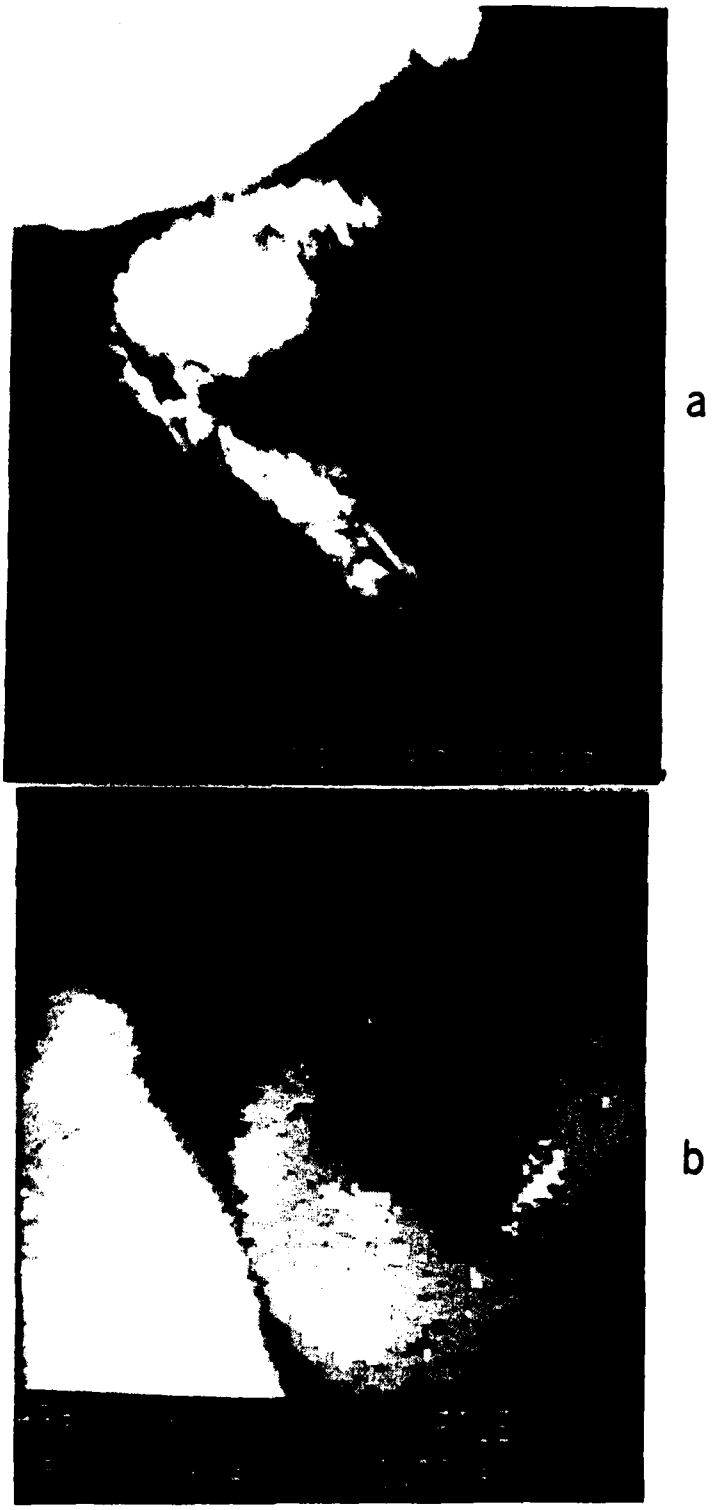

Figure 13. STEM micrographs of a spherical element similar to those of Figure 12. The hole and the thin areas of the sample are lighter in color; (a) scanning transmission micrograph, and (b) computer enhanced image.

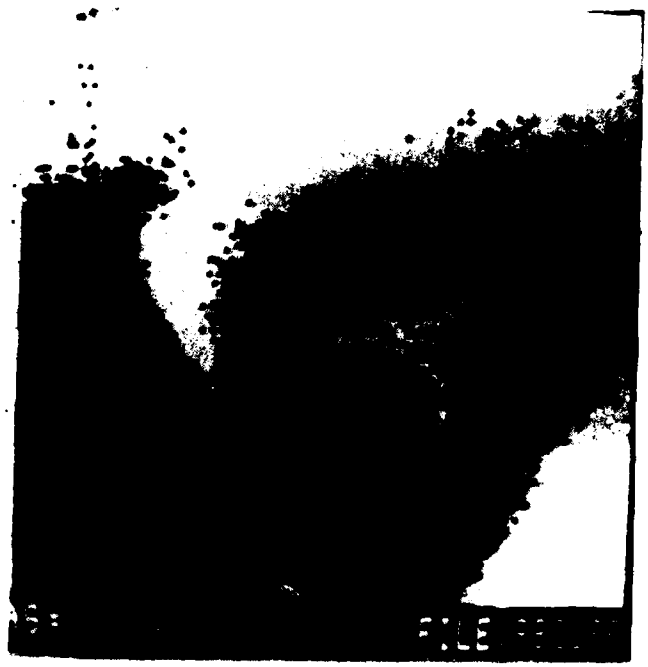

a

b

Figure 14. (a) Iron and (b) nickel K α x-ray map of the cell shown in Figure 13. The lighter colored regions indicate higher intensity signals.

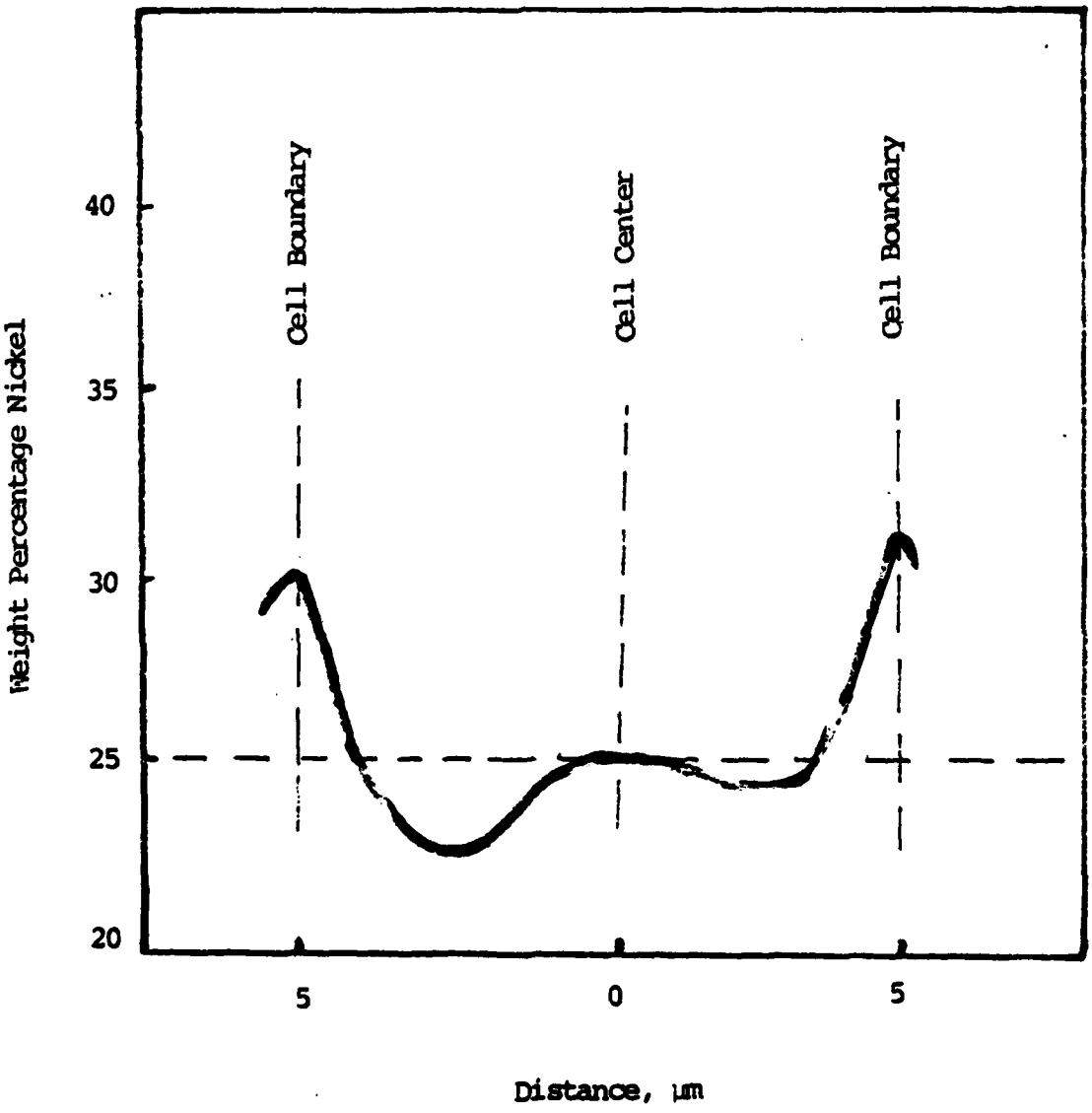

Figure 15. Approximate compositional profile across an element.

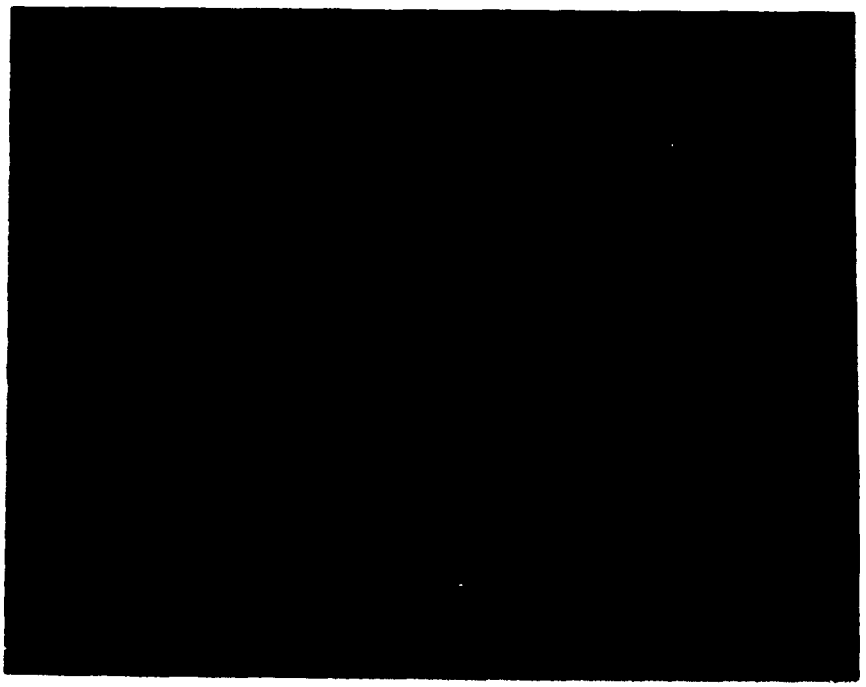

a

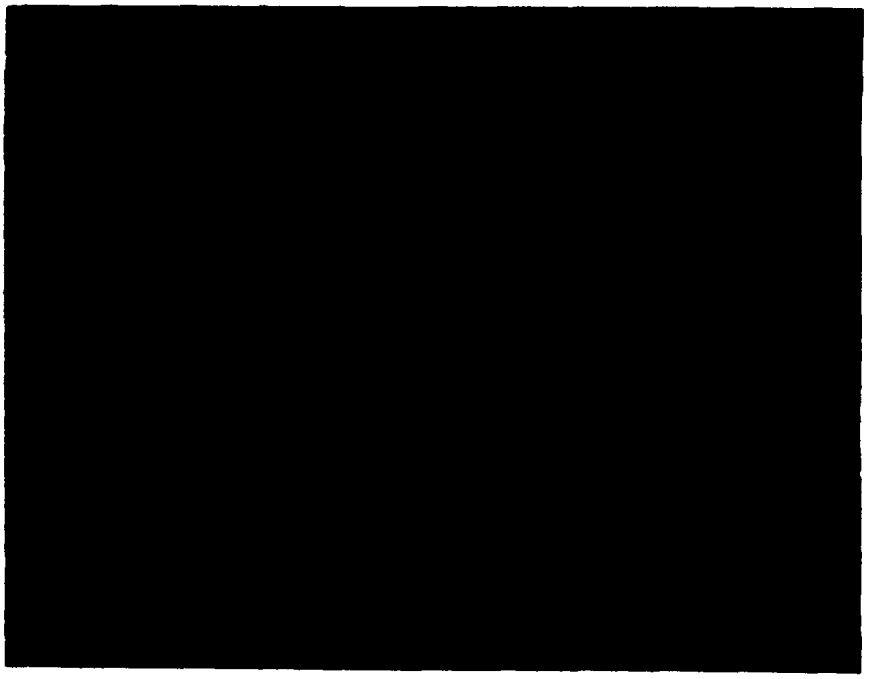

b

Figure 16. The grains structure of pure nickel at (a) 76 K and (b) 225 K supercooling. Magnification 50X.

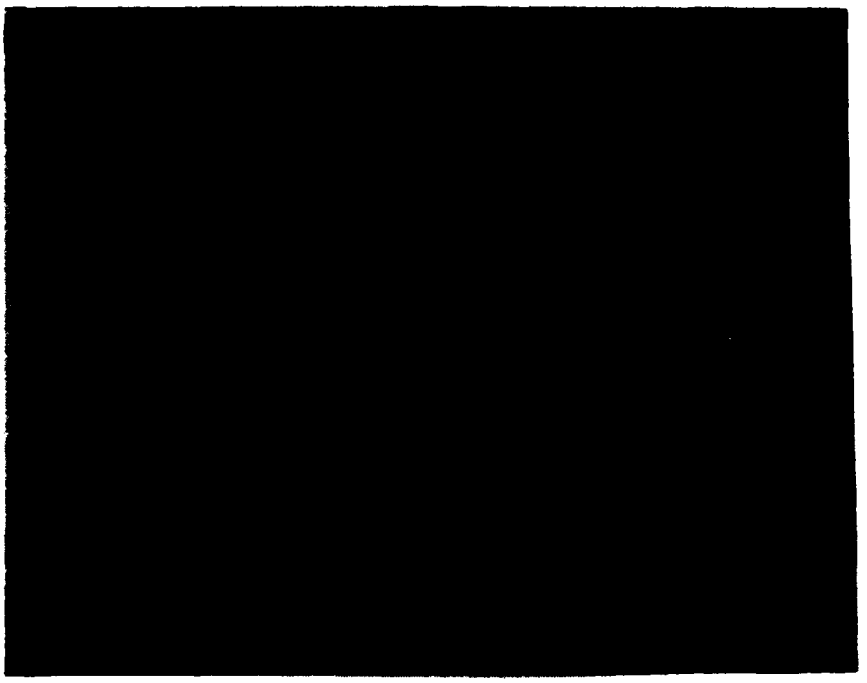

Figure 17. Grain structure of nickel supercooled 305 K. Magnification 100X.

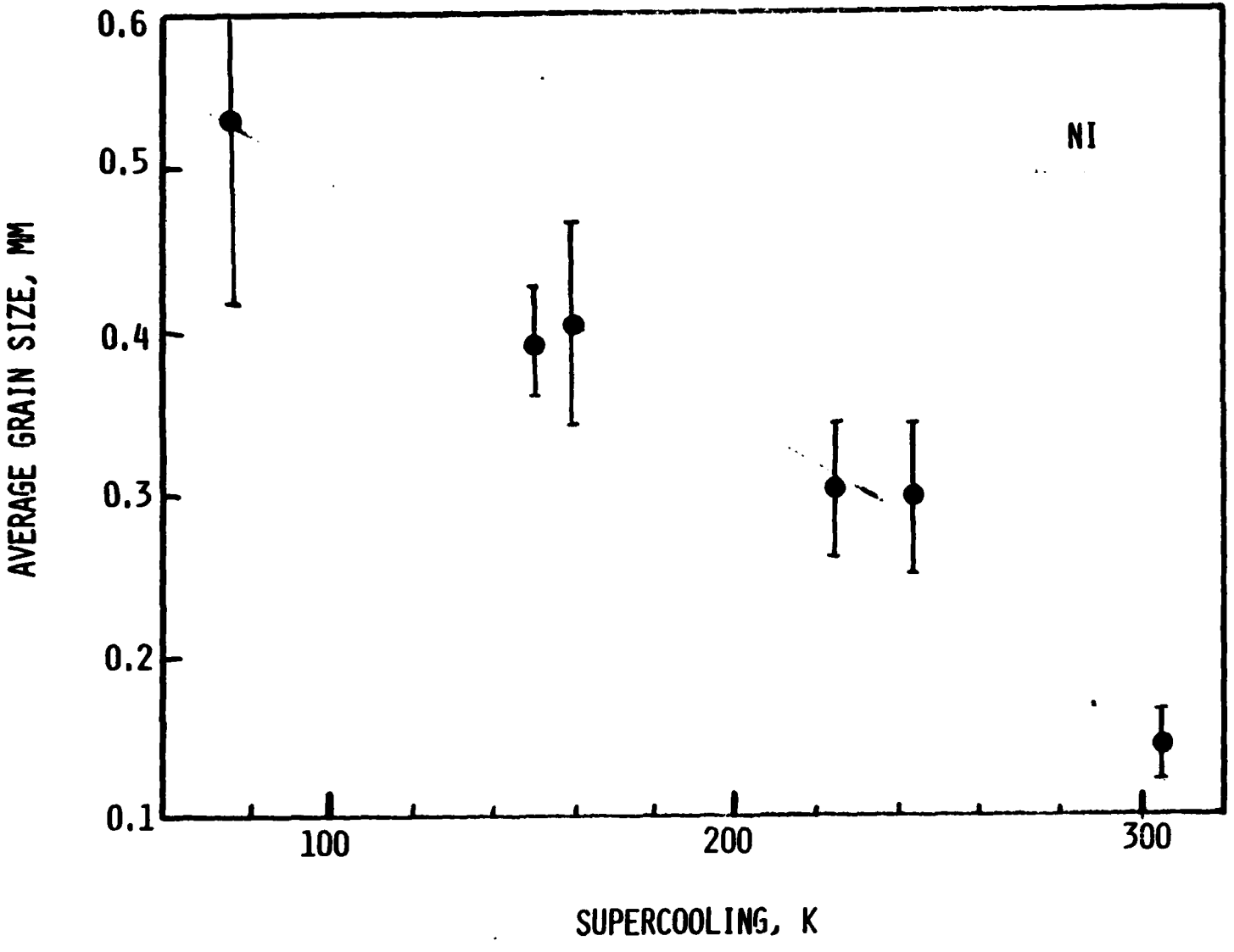

Figure 18. Effect of supercooling on the average grain size of nickel samples quenched in water.

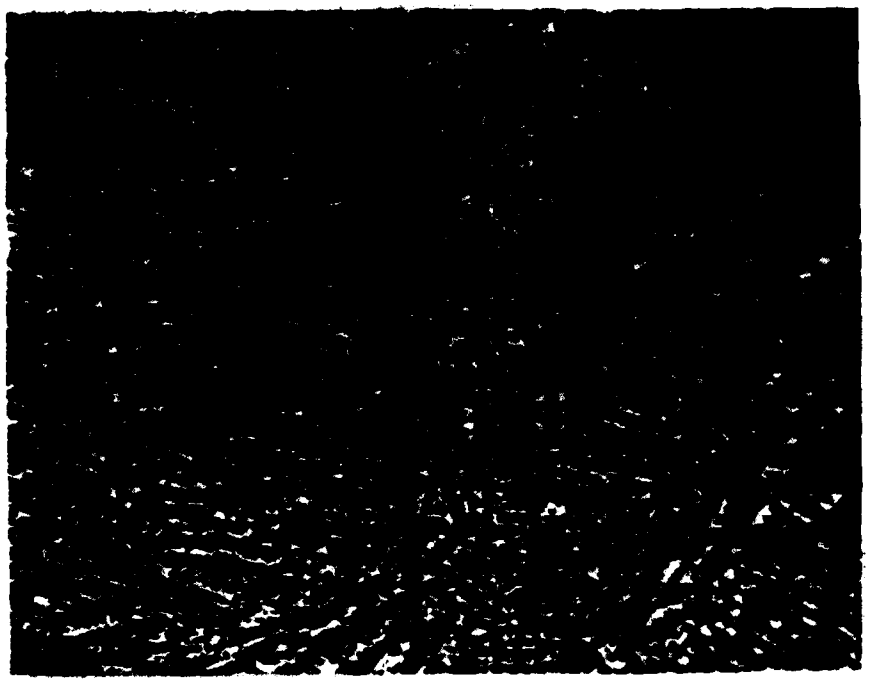

a

b

Figure 19. Dendritic-structure in two fully liquid 60 Cr-40 Ni samples quenched in water (a) at the liquidus temperature and (b) at 10 K supercooling below the liquidus. Magnification 200X.

Figure 20. Microstructure of a 60 Cr-40 Ni sample which had solidified at the levitated state prior to quenching in water. Magnification 200X.

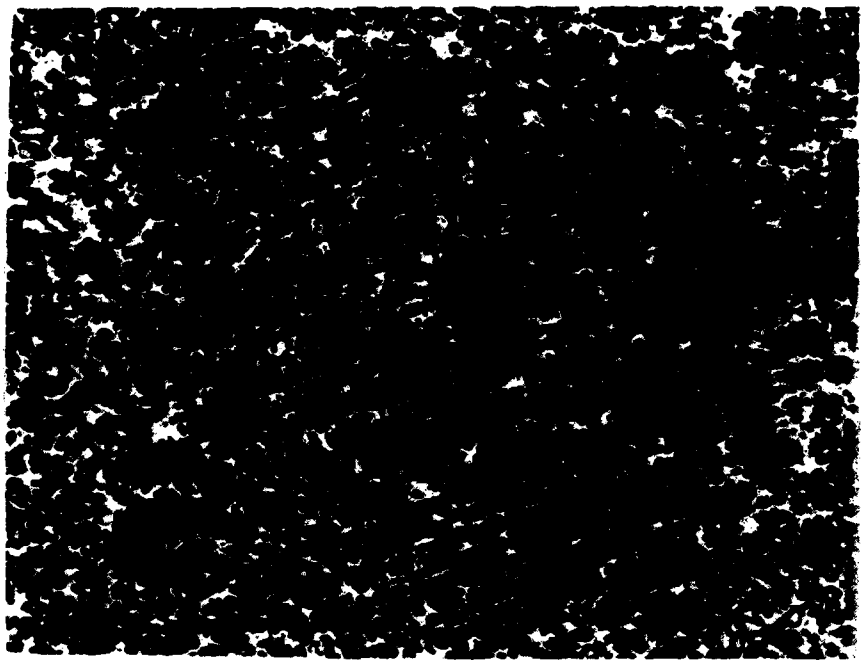

Figure 21. Microstructure of a 60 Cr-40 Ni sample quenched at the solid plus liquid range with 15-28 K supercooling below the solidus temperature. Magnification 200X.